

The continuous spectrum of bound states in expulsive potentials

Hidetsugu Sakaguchi¹, Boris A. Malomed², Andreas C. Aristotelous³ and Efstrathios G. Charalampidis⁴

¹Interdisciplinary Graduate School of Engineering Sciences,

Kyushu University, Kasuga, Fukuoka 816-8580, Japan

²Department of Physical Electronics, School of Electrical Engineering,

Faculty of Engineering, and Center for Light-Matter Interaction,

Tel Aviv University, P.O. Box 39040 Tel Aviv, Israel

³Department of Mathematics, The University of Akron, OH 44325, USA

⁴Department of Mathematics and Statistics and Computational Science Research Center,

San Diego State University, San Diego, CA 92182-7720, USA

On the contrary to the common intuition that a steep expulsive potential makes quantum states widely delocalized, we demonstrate that one- and two-dimensional (1D and 2D) Schrödinger equations, which include expulsive potentials that are *steeper than the quadratic* (anti-harmonic-oscillator) ones, give rise to *normalizable* (effectively localized) eigenstates. These states constitute full continuous spectra in the 1D and 2D cases alike. In 1D, these are spatially even and odd eigenstates. The 2D states may carry any value of the vorticity (alias magnetic quantum number). Asymptotic approximations for wave functions of the 1D and 2D eigenstates, valid far from the center, are derived analytically, demonstrating excellent agreement with numerically found counterparts. Special exact solutions for vortex states are obtained in the 2D case. These findings suggest an extension of the concept of bound states in the continuum, in quantum mechanics and paraxial photonics. Gross-Pitaevskii equations are considered as the nonlinear extension of the 1D and 2D settings. In 1D, the cubic nonlinearity slightly deforms the eigenstates, maintaining their stability. On the other hand, the quintic self-focusing term, which occurs in the photonic version of the 1D model, initiates the dynamical collapse of states whose norm exceeds a critical value.

I. INTRODUCTION

The separation of discrete and continuous spectra, which represent bound and delocalized states, respectively, is an underlying principle of the classical Sturm - Liouville theory [1, 2] and quantum mechanics, whose mathematical framework is based in this theory [3–5]. The fact that, in the paraxial approximation, the fundamental propagation equation for optical waves is tantamount to the quantum-mechanical Schrödinger equation makes the separation of discrete and continuous spectra an equally important tenet of optics and photonics [6–8]. Actually, this principle applies to various other physical settings modeled by equations of the Schrödinger type [9, 10].

Nevertheless, there are well-known exceptions from the separation principle, in the form of *bound states embedded in the continuum* (often designated by the BIC acronym). The first example was discovered in 1929 by von Neumann and Wigner (vNW) [11], solving the three-dimensional (3D) Schrödinger equation with the isotropic *expulsive* potential (written in a scaled form),

$$U(r) = \frac{1}{r^2} - \frac{9}{2}r^4. \quad (1)$$

This potential supports a normalizable BIC stationary wave function,

$$\varphi_{\text{vNW}}(r) = \frac{1}{r^2} \sin(r^3), \quad (2)$$

which corresponds to the zero energy eigenvalue. Later, schemes were designed for the realization of BIC states in semiconductor heterostructures [12–14]. Then, much interest was drawn to BIC modes in various photonic setups, where they offer a considerable potential for applications [15–19].

In the framework of the mean-field approximation, the linear Schrödinger equation for a single atom is closely related to its nonlinear version in the form of the Gross-Pitaevskii equation (GPE), which includes the cubic term accounting for the averaged effect of inter-atomic collisions in the Bose-Einstein-condensate (BEC) phase of ultracold atomic gases [21]. In the optical realization, a model similar to GPE is provided by the nonlinear Schrödinger equation (NLSE), which adds the Kerr self-focusing term to the paraxial propagation equation [6]. Under special conditions, NLSE-based optics models give rise to nonlinear states in the form of *embedded solitons*, which, similar to the BIC modes produced by the linear Schrödinger equation, may exist as peculiar localized states *embedded* in the continuous spectrum [22].

Another counter-intuitive species of bound states is produced by a system of two linearly coupled 1D or 2D equations, each one being either a linear or nonlinear Schrödinger equation, with the usual trapping harmonic-oscillator (HO)

potential in one equation, and the *expulsive* (anti-HO) potential in the other [23]. The 2D linear system for wave functions u and v , written in the polar coordinates (r, θ) , is

$$i\frac{\partial u}{\partial t} + \frac{1}{2} \left(\frac{\partial^2}{\partial r^2} + \frac{1}{r} \frac{\partial}{\partial r} - \frac{1}{r^2} \frac{\partial^2}{\partial \theta^2} \right) u + \lambda v - \frac{1}{2} r^2 u = -\omega u, \quad (3)$$

$$i\frac{\partial v}{\partial t} + \frac{1}{2} \left(\frac{\partial^2}{\partial r^2} + \frac{1}{r} \frac{\partial}{\partial r} - \frac{1}{r^2} \frac{\partial^2}{\partial \theta^2} \right) v + \lambda u + \frac{1}{2} \kappa r^2 v = 0, \quad (4)$$

where λ is the coefficient of the linear coupling, $\kappa > 0$ is the relative strength of the anti-HO potential, while the HO strength in Eq. (3) is fixed to be 1 by scaling, and ω represents a possible eigenvalue mismatch between the coupled equations. It was found [23] that the system of Eqs. (3) and (4) admits bound-state solutions, in the form of

$$\{u, v\} = \exp(-iEt + iS\theta) \{U(r), V(r)\}, \quad (5)$$

with integer vorticity $S = 0, 1, 2, \dots$, real eigenvalue E (alias the chemical potential, in terms of BEC), which is a function of the system's parameters λ , ω , κ and vorticity S (as a special example, see Eq. (8) below), and stationary real wavefunctions are localized as usual eigenstates of the 2D HO, i.e., $\{U(r), V(r)\} \sim r^S \exp(-r^2/2)$ at $r \rightarrow \infty$, despite the presence of the expulsive potential in Eq. (4). In particular, if the system's parameters are subject to the constraint $\omega = (1/2)(5 + S - \lambda^2)$, the bound state is found as an exact solution,

$$u = U_0 [(\lambda^2 - 1 - S) + r^2] r^S \exp\left(-iE_{\text{exact}} t + iS\theta - \frac{r^2}{2}\right), \quad (6)$$

$$v = -2\lambda U_0 r^S \exp\left(-iE_{\text{exact}} t + iS\theta - \frac{r^2}{2}\right), \quad (7)$$

with the eigenvalue given by

$$E_{\text{exact}} = \frac{1}{2} (\lambda^2 + 1 + S) \quad (8)$$

and with U_0 being an arbitrary amplitude. These strongly localized states, which exist with the single eigenvalue E , also represent BIC, as the same system gives rise to the continuous spectrum of weakly delocalized eigenstates, which are similar to the one given by Eq. (25) below.

The subject of the present work is to construct eigenstates of 1D and 2D linear and nonlinear Schrödinger equations (alias GPEs) with expulsive potentials, taken as the anti-HO term ($\gamma = 1$ in Eq. (9)) or steeper ones ($\gamma > 1$; note that the vNW example (1) includes $\gamma = 2$). The respective 1D GPE for wave function $\psi(x, t)$ is introduced, in the scaled form, as

$$i\frac{\partial \psi}{\partial t} = -\frac{1}{2} \frac{\partial^2 \psi}{\partial x^2} - \frac{1}{2} x^{2\gamma} \psi + g|\psi|^{2\sigma} \psi, \quad (9)$$

where the coefficient in front of the potential term is fixed by means of scaling (cf. Eq. (3)), $g = -1, 0, +1$ correspond to the self-focusing, zero, or defocusing nonlinearity, and two relevant values, $\sigma = 2$ and 4 , represent, respectively, the cubic and quintic self-interaction. The cubic nonlinearity is commonly known as the most generic one [6], while the quintic self-focusing, which can be implemented [24, 25] and used [26–29] under well-controlled conditions in optics [24–26], is interesting as it gives rise to *Townes solitons* in 1D [30]. Eigenstates produced by Eq. (9) with real eigenvalue E are looked for in the usual form, $\psi(x, t) = \exp(-iEt) \varphi(x)$, with stationary real eigenfunction $\varphi(x)$ satisfying the equation

$$E\varphi = -\frac{1}{2} \frac{d^2 \varphi}{dx^2} - \frac{1}{2} x^{2\gamma} \varphi + g\varphi^{2\sigma+1}. \quad (10)$$

In the experiments with cold atoms, the expulsive anti-HO or steeper potential, in its 1D and 2D forms alike, can be readily imposed by a blue-detuned optical beam with the Gaussian or super-Gaussian transverse structure [31, 32]. Another possibility of the experimental realization of the 1D model represented by Eq. (9) may refer to a gas of small polar molecules carrying a permanent electric dipole moment, cr. Refs. [33, 34]. Although this realization may seem too complex, one can consider the molecular gas loaded into a quasi-1D pipe-shaped optical trap, aligned with the x -axis, the dipoles being polarized in the positive and negative directions at $x > 0$ and $x < 0$, respectively, by a strong uniform electric field generated by a uniformly charged sheet placed at $x = 0$ perpendicular to the x -axis. The

expulsive potential $\sim 1/x^2$ ($\gamma = 1$ in Eq. (9)) is then imposed by a point-like charge additionally placed at $x = 0$, with the sign opposite to that of the polarizing sheet.

One may intuitively expect that the strongly expulsive potential in Eq. (9) leads to strong delocalization of the respective eigenstates. Nevertheless, we demonstrate, analytically and numerically, that the intuition is misleading: the 1D and 2D linear Schrödinger equations with the anti-HO potential, $\gamma = 1$, give rise to weakly delocalized states (whose norm diverges logarithmically with the increase of the spatial size), while all steeper expulsive potentials, corresponding to $\gamma > 1$, produce *well-localized bound states* with a convergent norm, which form a *continuous spectrum* ($-\infty < E < +\infty$). This situation seems unusual in quantum mechanics.

While the most essential results are reported here in the framework of the 1D and 2D linear Schrödinger equations, numerical analysis demonstrates that the 1D bound states remain *completely stable* in the presence of the cubic term in Eq. (9) ($\sigma = 1$). The quintic self-focusing term ($\sigma = 2$ in Eq. (9), with $g = -1$) gives rise to the collapse of the 1D bound states if their norm exceeds a certain critical value, while they are stable below the critical level. This situation is typical for the Townes-soliton phenomenology [35–38].

Analytical and numerical results for the bound states in the 1D linear Schrödinger equation are reported in Section 2. This is followed by a brief consideration of nonlinear bound states and their stability in the framework of the 1D NLSEs with the cubic and quintic self-focusing terms ($g = -1$ and $\sigma = 1$ or 2, in terms of Eq. (9)), in Section 3. Findings for the 2D bound states, including vortex ones, which carry the angular momentum, are presented in Section 4 (chiefly, for the linear Schrödinger equation). In particular, the consideration of the 2D linear Schrödinger equation with the expulsive potential produces exact solutions for the vortex states, under a special constraint imposed on the model's parameters. The paper is concluded by Section 5.

II. ONE-DIMENSIONAL LINEAR BOUND STATES

The starting point of the analysis is the linear version ($g = 0$) of the 1D stationary equation (10). While the equation is not an analytically solvable one, it is straightforward to construct its asymptotic solution, valid for sufficiently large values of $|x|$ and $\gamma > 1$:

$$\varphi_{\text{asympt}}^{(1D)}(x; \gamma > 1; E) = \varphi_0 |x|^{-\gamma/2} \cos \left(\frac{|x|^{\gamma+1}}{\gamma+1} - \chi_0 \right) + \frac{E\varphi_0}{\gamma-1} |x|^{-3\gamma/2+1} \sin \left(\frac{|x|^{\gamma+1}}{\gamma+1} - \chi_0 \right), \quad (11)$$

where φ_0 and χ_0 are arbitrary constants, in terms of the asymptotic expansion (note that setting $\gamma = 1/2$ in the first term in Eq. (11) reproduces the well-known asymptotic form of the Airy function [3]). The approximation (11) retains the first two terms of the expansion, while its third-order correction (TOC) reads

$$\text{TOC} \left(\varphi_{\text{asympt}}^{(1D)}(x); \gamma > 1 \right) = \frac{1}{8} \frac{\gamma(\gamma+2)}{\gamma+1} \varphi_0 |x|^{-3\gamma/2-1} \sin \left(\frac{|x|^{\gamma+1}}{\gamma+1} - \chi_0 \right). \quad (12)$$

The obvious property of Eq. (11) is the *convergence* of its integral norm, $N = \int_{-\infty}^{+\infty} \varphi^2(x) dx$ at $|x| \rightarrow \infty$, for $\gamma > 1$ and all eigenvalues (the full spectrum), $-\infty < E < +\infty$. Thus, we arrive at a simple but counter-intuitive conclusion: any expulsive potential which is *steeper* than the anti-HO one ($\gamma > 1$) produces *normalizable* bound states, which populate the full continuous spectrum. Qualitatively, this conclusion can be explained by noting that a classical counterpart of the quantum particle would be rolling down the steep potential hill with rapidly growing acceleration, which gives rise to the strongly oscillating phase of the respective wave function, the latter feature leading to the *effective localization* (normalizability) of the eigenstate.

Note that all inflection points ($d^2\varphi/dx^2 = 0$) of the stationary wave function produced by Eq. (10) with $g = 0$ and $E \geq 0$ coincide with zero-crossing ones, $\varphi(x) = 0$. In the case of $E < 0$, there are two additional inflection points, *viz.*, $x = \pm (-2E)^{1/(2\gamma)}$.

The situation is different in the case of the anti-HO potential, with $\gamma = 1$ in Eq. (9). In this case, the approximation (11) is valid solely for $E = 0$, yielding $\varphi_{\text{asympt}}^{(1D)}(x; \gamma = 1; E = 0) = \varphi_0 |x|^{-1/2} \cos(x^2/2 - \chi_0)$, demonstrating that the respective normalization integral slowly diverges,

$$N \simeq \varphi_0^2 \ln(L/l), \quad (13)$$

where $2L$ is the size of the integration domain, and l is a characteristic scale of the inner core of the wave function. For $E \neq 0$, the correct asymptotic approximation takes the form of

$$\varphi_{\text{asympt}}^{(1D)}(x; \gamma = 1; E) = \varphi_0 |x|^{-1/2} \cos \left(\frac{x^2}{2} + E \ln \left(\frac{|x|}{l} \right) \right), \quad (14)$$

whose norm diverges as in Eq. (13).

The wave function of the 1D eigenstate, produced by a numerical solution of Eq. (10) with $g = 0$, $\gamma = 1$ and $E = 0$, and its comparison to the asymptotic approximation (11), are plotted in Fig. 1, with fitting constants $\chi_0 = \pi/8$ and $\varphi_0 = 1$ in Eq. (11) (the latter value is actually arbitrary for the linear solution). It is clearly observed that the asymptotic approximation provides high accuracy, in comparison to its numerical counterpart.

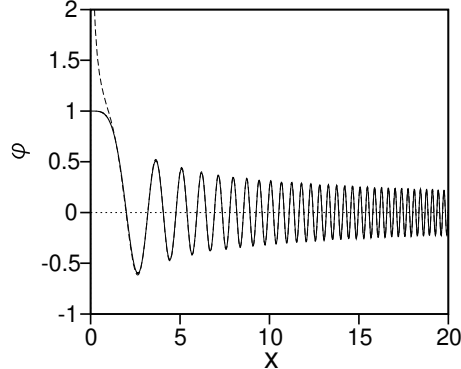


FIG. 1. The continuous curve: a numerically found spatially even solution of Eq. (10) with $g = 0$, $\gamma = 1$ (the anti-HO expulsive potential) and $E = 0$. The dashed curve: the asymptotic approximation (11) for the same solution, with fitting constants $\chi_0 = \pi/8$ and $\varphi_0 = 1$.

In Fig. 1, and similar in the numerically generated plots presented below, it is not easy to display far tails, as the rapidly accelerating phase oscillations in Eq. (11) imply that the accurate numerical solution must take into regard spatial harmonics of very high orders. On the other hand, the asymptotic expression (11) yields the tails in the virtually exact analytical form.

A typical example of the 1D bound state for $\gamma = 2$ (the quartic expulsive potential), produced by the numerical solution of Eq. (10), and its comparison to the asymptotic approximation (11), is displayed in Fig. 2. In this case too, the asymptotic approximation demonstrates remarkably high accuracy.

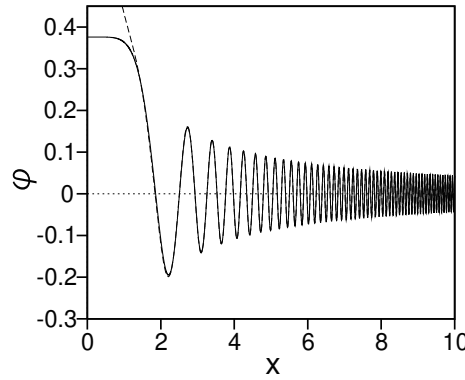


FIG. 2. The continuous curve: a numerically found spatially even solution of Eq. (10) with $g = 0$, $\gamma = 2$ (the quartic expulsive potential) and $E = 0$. The dashed curve: the asymptotic approximation (11) for the same case, with fitting constants $\chi_0 = \pi/6$ and $\varphi_0 = 0.44$.

Note: For visualization purposes, the wavefunctions in several numerical figures were vertically rescaled. Accordingly, the plotted amplitudes do not represent the original normalization of the stationary solutions, and any amplitude-related fitting parameters (such as φ_0) correspond to the rescaled profiles shown in the plots.

For given E , the asymptotic-tail expressions (11) and (12) may belong, at least, to two different global solutions (full eigenstates), *viz.*, the *fundamental* spatially even one, with $\varphi(-x) = \varphi(x)$ (alias the ground state, for given E), and the *dipole* spatially odd eigenstate, with $\varphi(-x) = -\varphi(x)$ (alias the first excited state). To illustrate this possibility for the same cases as considered above for the fundamental solutions, *viz.*, $\gamma = 1$ and $\gamma = 2$, the corresponding numerically found dipole eigenstates, obtained with the boundary condition $d\varphi/dx|_{x=0} = 0$, are plotted in Figs. 3(a)

and (b), respectively. It is plausible that Eq. (10) may produce additional spatially even and odd solutions, which correspond to higher-order excited states in terms of quantum mechanics. This issue will be considered elsewhere.

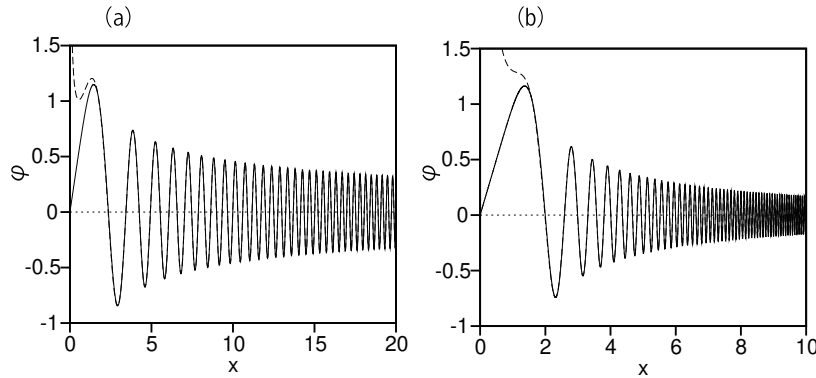


FIG. 3. In panels (a) and (b), the continuous curves represent numerically found spatially odd (dipole-mode) solutions of Eq. (10) with $g = 0$ and $E = 0$, for $\gamma = 1$ and 2 , respectively (cf. their spatially even counterparts in Figs. 1 and 2). The dashed curves represent the corresponding asymptotic approximation (11) with fitting constants $\chi_0 = 3\pi/8$, $\varphi_0 = 1.45$ in (a), and $\chi_0 = \pi/3$, $\varphi_0 = 1.72$ in (b).

While the above examples display eigenstates found with the zero eigenvalue ($E = 0$), Fig. 4 presents a typical eigenstate for a very large negative eigenvalue, *viz.*, $E = -200$, in the case of $\gamma = 2$ (the quartic expulsive potential). It is seen that the large value of $-E$ suppresses the wave function in the core area of the eigenstate. As the energy decreases, the wave function goes away from the potential maximum around $x = 0$. As $E \rightarrow -\infty$, $x_{\max} \rightarrow \infty$ and the wave function approaches the ground state. At the edge of the core, the wave function quickly grows towards the largest value, attained at a point with $|x| = x_{\max}$, as $\varphi(x) \sim \exp(\sqrt{-2E}(x - x_{\max}))$, in agreement with Eq. (10). This is followed by the gradual decay of the rapidly oscillating tail, as per Eq. (11). The dependence of x_{\max} on $|E|$ may be predicted, in a crude approximation, by equating the two respective large terms in Eq. (10), i.e., $-E\varphi \sim (1/2)x_{\max}^4\varphi$, hence, in the logarithmic approximation,

$$\ln(x_{\max}) \simeq (1/4)\ln(-E). \quad (15)$$

This simple relation is compared to the numerical data in Fig. 5.

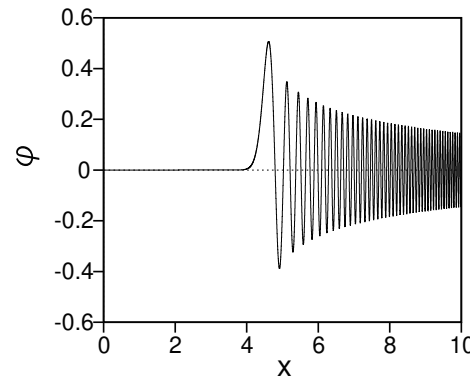


FIG. 4. The spatially even eigenstate produced by the numerical solution of Eq. (10) with $g = 0$, $\gamma = 2$, and $E = -200$.

In the eigenstates corresponding to very large positive eigenvalues, the core area, $|x| \lesssim E^{1/4}$, is not (nearly) empty, unlike Fig. 5. Instead, it is filled by a uniform standing wave, $\varphi(x) \approx \varphi(x = 0) \cos(\sqrt{2E}x)$ (not shown here in detail).

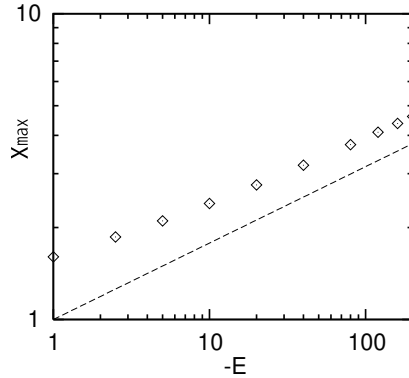


FIG. 5. The numerically found dependence of the coordinate x_{\max} , at which the wave function attains the largest value, on the eigenvalue $E < 0$, for $g = 0$ and $\gamma = 2$. The dependence is plotted on the log-log scale, with the straight dashed line corresponding to the approximate relation (15).

III. BOUND STATES IN THE 1D NONLINEAR SCHRÖDINGER EQUATION (NLSE) WITH THE EXPULSIVE POTENTIAL

While the stability of the existing eigenstates in the framework of the linear Schrödinger equation is obvious, it is a nontrivial problem in the case of the NLSE. Numerical simulations of the perturbed evolution of bound states produced by Eq. (9) with the cubic nonlinearity, $\sigma = 1$ and $g = \pm 1$, has demonstrated that all the respective bound states remain stable, while their stationary shape is slightly deformed by the cubic term. A typical example of the stable evolution of the bound state for $g = -1$ (the self-focusing cubic term), $\gamma = 2$ (the quartic expulsive potential), and $E = -1$ is presented in Fig. 6.

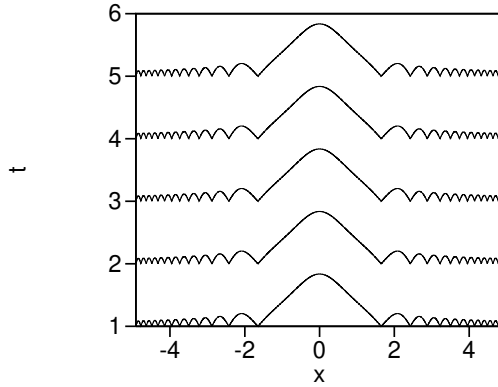


FIG. 6. The stable evolution of the spatially even eigenstate obtained as the numerical solution of Eq. (10) with $\gamma = 2$, $g = -1$, $\sigma = 1$ (the cubic self-focusing term), and $E = -1$. The norm of the eigenstate is $N = 2.86$.

The 1D spatially odd (dipole) eigenstates also remain stable, being only weakly deformed by the cubic nonlinearity. An example is displayed in Fig. 7 for $\gamma = 2$, $\sigma = 1$, $g = +1$ (the self-defocusing cubic term) and $E = 0$, i.e., the same parameters as those (except for $g = 0$) of the dipole-mode eigenstate shown in Fig. 3(b), which was produced by the linear version of Eq. (10). Note that both eigenstates are very well approximated by the asymptotic expression (11) with appropriate values of the fitting constants, *viz.*, $\chi_0 = \pi/3$ for $g = 0$ and $\chi_0 = 5\pi/12$ for $g = +1$.

In the case of the quintic self-focusing, which corresponds to $g = -1$ and $\sigma = 2$ in Eq. (9), the eigenstate whose norm exceeds a certain critical value is unstable against the onset of the collapse. This point will be reported in detail elsewhere.

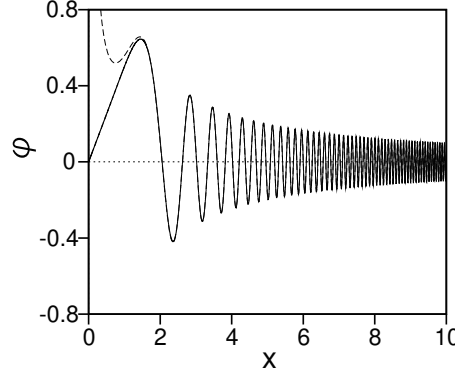


FIG. 7. The stable spatially odd eigenstate produced by the numerical solution of Eq. (10) with $g = +1$, $E = 0$, and $\gamma = 2$, cf. its counterpart plotted in Fig. 3(b) produced for the same parameters by the linearized equation (with $g = 0$). The norm of eigenstate is $N = 1.23$. The dashed curve represents the corresponding asymptotic approximation (11) with fitting constants $\chi_0 = 5\pi/12$ and $\varphi_0 = 0.995$.

IV. TWO-DIMENSIONAL BOUND STATES

The natural 2D version of Eq. (9) can also be realized experimentally as the GPE for ultracold atoms, under the action of the isotropic expulsive optical potential, induced by the blue-detuned laser beam. In terms of the polar coordinates (r, θ) , the 2D GPE is written as

$$i\frac{\partial\psi}{\partial t} = -\frac{1}{2}\left(\frac{\partial^2\psi}{\partial r^2} + \frac{1}{r}\frac{\partial\psi}{\partial r} + \frac{1}{r^2}\frac{\partial^2\psi}{\partial\theta^2}\right) - \frac{1}{2}r^{2\gamma}\psi + g|\psi|^2\psi, \quad (16)$$

with $\gamma \geq 1$ (here, only the cubic nonlinear term is considered, if any). The stationary version of Eq. (16) with vorticity S (alias magnetic quantum number) and eigenvalue E (the chemical potential, in terms of the BEC), is produced by the substitution

$$\psi = \exp(-iEt + iS\theta)\varphi(r), \quad (17)$$

where real function $\varphi(r)$ obeys the equation

$$E\varphi = -\frac{1}{2}\left(\frac{d^2\varphi}{dr^2} + \frac{1}{r}\frac{d\varphi}{dr} - \frac{S^2}{r^2}\varphi\right) - \frac{1}{2}r^{2\gamma}\varphi + g\varphi^3. \quad (18)$$

Similar to Eq. (11) in the 1D case, it is straightforward to construct the asymptotic form of the tail of the solution to Eq. (18) at $r \rightarrow \infty$, in the case of $\gamma > 1$. The first two terms of the asymptotic expansion are

$$\varphi_{\text{asympt}}^{(2D)}(r) = \varphi_0 r^{-(\gamma+1)/2} \cos\left(\frac{r^{\gamma+1}}{\gamma+1} - \chi_0\right) + \frac{E\varphi_0}{\gamma-1} r^{-(3\gamma-1)/2} \sin\left(\frac{r^{\gamma+1}}{\gamma+1} - \chi_0\right), \quad (19)$$

and the TOC term is

$$\text{TOC}\left(\varphi_{\text{asympt}}^{(2D)}(x)\right) = \varphi_0 \frac{(\gamma+1)^2 - 4S^2}{2(2\gamma+1)} r^{-3(\gamma+1)/2} \sin\left(\frac{r^{\gamma+1}}{\gamma+1} - \chi_0\right), \quad (20)$$

cf. its 1D counterpart (12). As above, φ_0 and χ_0 are indefinite constants, in the framework of the asymptotic expansion at $r \rightarrow \infty$. Note that only the smallest asymptotic term (20) includes the vorticity.

As seen from expression (19), the 2D norm of these eigenstates, $N_{2D} = 2\pi \int_0^\infty \varphi^2(r)rdr$, converges under precisely the same condition as in 1D, *viz.*, $\gamma > 1$, i.e., if the 2D expulsive potential is *steeper* than the isotropic anti-HO potential. A qualitative explanation for this counter-intuitive conclusion is the same as in the 1D setting: under the action of the expulsive potential, a classical particle would be rolling down the steep potential hill (along a spiral trajectory, if the particle carries the angular momentum, corresponding to $S \geq 1$), with rapid acceleration. In terms of the particle's quantum counterpart, the acceleration gives rise to the strongly oscillating phase in the wave function, thus leading to the normalizability (effective localization) of the eigenstate.

Similar to the 1D case, the 2D Schrödinger equation (16) with $\gamma = 1$, the asymptotic expression (19) is relevant solely for $E = 0$, as otherwise the second term diverges. For $E \neq 0$, the relevant asymptotic approximation is

$$\varphi_{\text{asympt}}^{(2D)}(r) = \varphi_0 r^{-1} \cos \left(\frac{r^2}{2} + E \ln \left(\frac{r}{l} \right) \right), \quad (21)$$

where l is the radius of the inner core, cf. Eq. (14). Also similar to its 1D counterpart, in the case of $\gamma = 1$ the norm of the 2D eigenstate is slowly diverging, $N_{2D} \simeq \pi \varphi_0^2 \ln(L/l)$ (cf. Eq. (13)), where L is the radius of the integration domain.

An additional analytical result, which is not available in the 1D case, is the existence of particular *exact solutions* to the linear version Eq. (18), with $g = 0$ and $E = 0$, if the power factor γ of the explosive potential in Eq. (16) is selected, for given integer vorticity $S \geq 1$, as

$$\gamma(S) = 2S - 1. \quad (22)$$

In this case, the exact wave function is

$$\varphi_{\text{exact}}(r; S) = \frac{\varphi_0}{r^S} \sin \left(\frac{r^{2S}}{2S} \right), \quad (23)$$

where φ_0 is an arbitrary amplitude (the correctness of solution (23) was also checked by comparing to its numerically constructed counterpart).

For all integer values $S \geq 2$, the norm of the exact wave function (23) converges, yielding

$$(N_{2D})_{\text{exact}} = 2\pi \int_0^\infty \varphi_{\text{exact}}^2(r; S) r dr = \varphi_0^2 \frac{\pi \Gamma(1/S)}{2S^{1-(1/S)} (S-1)} \cos \left(\frac{\pi}{2} \left(1 - \frac{1}{S} \right) \right). \quad (24)$$

where $\Gamma(1/S)$ is the Gamma-function. In agreement with the above conclusion, the norm diverges for $\gamma = 1$, i.e., $S = 1$, see Eq. (22), the respective exact solution (23) taking the form of

$$\varphi_{\text{exact}}(r; S = 1) = \frac{\varphi_0}{r} \sin \left(\frac{r^2}{2} \right). \quad (25)$$

This solution is plotted in Fig. 8.

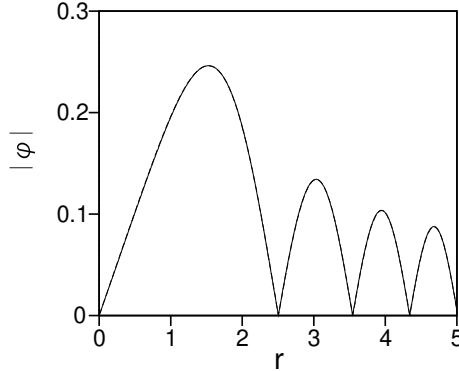


FIG. 8. The absolute value $|\varphi(r)|$ of the exact solution (25) of Eq. (18) with $\gamma = 1$, $g = 0$, $S = 1$, and $E = 0$.

Lastly, if the cubic term is retained in Eq. (18), one can construct an approximate solution for $E = 0$ and $S \neq 1$, neglecting the third harmonic in the elementary formula $\sin^3 \Phi = (3/4) \sin \Phi - (1/4) \sin(3\Phi)$. The approximate solution is given by Eq. (25) (even if S is not 1), in which the amplitude is determined by the balance of the linear and nonlinear terms in Eq. (18):

$$\varphi_0^2 = -2(3g)^{-1} (S^2 - 1). \quad (26)$$

Thus, the approximate solution (25) of Eq. (18) with the self-defocusing or focusing nonlinearity, i.e., $g = +1$ or $g = -1$, exists, yielding $\varphi_0^2 > 0$ as per Eq. (26), for $S = 0$ or $S \geq 2$, respectively.

In the case of $g = -1$ (self-focusing), it is necessary to test the stability of the nonlinear vortex solutions against spontaneous splitting, cf. Refs. [39–42]. These results will be reported elsewhere.

V. CONCLUSION

Our analysis demonstrates that, on the contrary to the intuitive expectation, the 1D and 2D Schrödinger equations with the expulsive potential which is steeper than the anti-HO (anti-harmonic-oscillator) one, generates a full continuous spectrum of the normalizable bound states. In 1D these may be fundamental and dipole modes (spatially even and odd ones, respectively; plausibly, higher-order excited states exist too, which is a subject for additional analysis). The 2D bound states may carry any integer vorticity (angular momentum). Universal asymptotic expressions for the 1D and 2D states, valid at $|x| \rightarrow \infty$ and $r \rightarrow \infty$, respectively, are found, providing an extremely accurate approximation to the numerically found wave functions. In addition, in the 2D case special vorticity-carrying solutions are found in the exact form. These results essentially extend the concept of BIC (bound states in the continuum), which has recently drawn much interest in the context of photonics, where the paraxial propagation models amount to the same Schrödinger equations as in quantum mechanics. In the limit of the anti-HO shape of the expulsive potential, the respective normalization integrals are weakly divergent, in 1D and 2D settings alike. The nonlinear version of the 1D and 2D models, in the form of the respective GPEs (Gross-Pitaevskii equations), are considered too. In 1D, the cubic self-focusing or defocusing nonlinearity slightly deforms the linear solutions and does not break their stability. The quintic self-focusing term makes the 1D bound states unstable against the onset of the collapse if the norm of the state exceeds the critical value.

As the further extension of the present work, it may be relevant to develop the analysis of the 2D model with the cubic nonlinear term. In particular, a challenging issue is the (in)stability of the nonlinear vortex eigenstates against spontaneous splitting by the azimuthal modulational instability in the case of the self-focusing sign of the nonlinearity, cf. works [39–42], in which a similar problem was investigated for nonlinear vortex states trapped in the usual isotropic HO potential. In parallel, and from the dynamical systems perspective, it may be relevant to perform a spectral stability analysis (in the realm of the Bogoliubov-de Gennes analysis) [43, 44] in order to track the states' spectrum and identify potential bifurcations. Finally, a true challenge while numerically computing such states herein is the need of using a large number of grid points for capturing the tails' oscillations as we observed in the present study. A potential way out for the 2D problem may be the use of mesh adaptation, see, e.g., [45] that will help resolving these oscillations very well with less computational cost. Those studies are underway and results will appear in future contributions.

VI. FUNDING

EGC acknowledges support from the San Diego State University, Department of Mathematics and Statistics startup fund. EGC thanks P.G. Kevrekidis for fruitful discussions during the early stages of this work.

VII. AUTHOR CONTRIBUTIONS

Software development and numerical calculations: H.S., A.C.A., and E.C. Analytical considerations: B.A.M. and H.S. Analysis of the results: all authors. Drafting the manuscript: B.A.M. H.S, and A.C.A.

VIII. CONFLICT OF INTERESTS

Authors declare no conflict of interests

IX. DATA AVAILABILITY STATEMENT

The data supporting the findings of this publication can be made available upon request.

[1] Courant R. and Hilbert D., *Methods of Mathematical Physics*. Vol. 1 (Wiley-VCH, Weinheim, 1953).
 [2] Zettl A., *Sturm-Liouville Theory* (AMS, Providence, 2005).
 [3] Landau L. D. and Lifshitz E. M., *Quantum Mechanics* (Nauka publishers, Moscow, 1974).
 [4] Bohm D., *Quantum Theory* (Dover, New York, 1989).

[5] Ballentine L. E., *Quantum Mechanics* (World Scientific, Singapore, 2000).

[6] Kivshar Y. S. and Agrawal G. P., *Optical Solitons: From Fibers to Photonic Crystals* (Academic Press, San Diego, 2003).

[7] Chen Z., Segev M., and Christodoulides D. N., Optical spatial solitons: historical overview and recent advances, *Rep. Prog. Phys.* **75**, 086401 (2012), doi:10.1088/0034-4885/75/8/086401.

[8] Gillen G. D., Gillen K., and Guha S., *Light Propagation in Linear Optical Media* (Taylor & Francis, Boca Raton, 2014).

[9] Yang J., *Nonlinear Waves in Integrable and Nonintegrable Systems* (SIAM, Philadelphia, 2010).

[10] Carretero-González, R., Frantzeskakis D. J., and Kevrekidis, P. G., *Nonlinear Waves & Hamiltonian Systems: From One To Many Degrees of Freedom, From Discrete To Continuum* (Oxford University Press, Oxford, 2024).

[11] von Neumann J. and Wigner E., Über merkwürdige diskrete Eigenwerte, *Phys. Z.* **30**, 465-467 (1929).

[12] Herrick, D. R., Construction of bound states in the continuum for epitaxial heterostructure superlattices, *Physica B* **85**, 44-50 (1976).

[13] Stillinger F. H., Potentials supporting positive-energy eigenstates and their application to semiconductor heterostructures, *Physica B* **85**, 270-276 (1976).

[14] Friedrich H. and Wintgen, D., Interfering resonances and bound states in the continuum, *Phys. Rev. A* **32**, 3231-3242 (1985).

[15] Marinica D. C., Borisov A. G., and Shabanov S. V., Bound states in the continuum in photonics, *Phys. Rev. Lett.* **100**, 183902 (2008).

[16] C. W. Hsu, Zhen B., Stone A. D., Joannopoulos J. D., and Soljačić M., Bound states in the continuum, *Nature Rev. Mat.* **9**, 16048 (2016).

[17] Kodigala A., Lepetit T., Gu Q., Bahari B., Fainman Y., and Kanté B., Lasing action from photonic bound states in continuum, *Nature* **541**, 196-199 (2017).

[18] Koshelev K., Lepeshov S., Liu M. K. Bogdanov A., and Kivshar, Asymmetric Metasurfaces with High-Q Resonances Governed by Bound States in the Continuum, *Phys. Rev. Lett.* **121**, 193903 (2018).

[19] Liu Z. J., Xu Y., Lin Y., Xiang J., Feng T. H., Cao Q. T., Li J. T., Lan S., and Liu J., High-Q Quasibound States in the Continuum for Nonlinear Metasurfaces, *Phys. Rev. Lett.* **123**, 253901 (2019).

[20] Koshelev K., Kruk S., Melik-Gaykazyan E., Choi J. H., Bogdanov A., Park H. G., and Kivshar Y., Subwavelength dielectric resonators for nonlinear nanophotonics, *Science* **367**, 288-292 (2020).

[21] Pitaevskii L. P. and Stringari S., *Bose-Einstein Condensation* (Oxford University Press, Oxford, 2003).

[22] Champneys A. R., Malomed B. A., Yang J., and Kaup D. J., “Embedded solitons”: solitary waves in resonance with the linear spectrum, *Physica D* **152-153**, 340-354 (2001).

[23] Hacker N. and Malomed B. A., Trapping wave fields in an expulsive potential by means of linear coupling, *Phys. Rev. E* **105**, 034213 (2022).

[24] Reyna A. S., Jorge K. C., and de Araújo C. B., Two-dimensional solitons in a quintic-septimal medium, *Phys. Rev. A* **90**, 063835 (2014).

[25] Reyna A. S. and de Araújo C. B., High-order optical nonlinearities in plasmonic nanocomposites – a review, *Adv. Opt. Phot.* **9**, 720-774 (2017).

[26] Quiroga-Teixeiro M. and Michinel H., Stable azimuthal stationary state in quintic nonlinear optical media, *J. Opt. Soc. Am. B* **14**, 2004-2009 (1997).

[27] Pego R. L. and Warchall H. A, Spectrally stable encapsulated vortices for nonlinear Schrödinger equations, *J. Nonlinear Sci.* **12**, 347-394 (2002).

[28] Sakaguchi H., Motion of pulses and vortices in the cubic-quintic complex Ginzburg-Landau equation without viscosity, *Physica D* **210**, 138-148 (2005).

[29] Skarka. V. and Aleksić N. B., Stability criterion for dissipative soliton solutions of the one-, two-, and three-dimensional complex cubic-quintic Ginzburg-Landau equations, *Phys. Rev. Lett.* **96**, 013903 (2006).

[30] Abdullaev F. Kh. and Salerno M., Gap-Townes solitons and localized excitations in low-dimensional Bose-Einstein condensates in optical lattices, *Phys. Rev. A* **72**, 033617 (2005).

[31] Boyer V., Godun R. M., Smirne G., Casettari D., Chandrashekar, C. M., Deb A. B., Laczik Z. J., and Foot C. J., Dynamic manipulation of Bose-Einstein condensates with a spatial light modulator, *Phys. Rev. A* **73**, 031402 (2006).

[32] Lin Y. J., Perry A. R., Compton, R. L., Spielman, I. B., and Porto J. V., Rapid production of ^{87}Rb Bose-Einstein condensates in a combined magnetic and optical potential, *Phys. Rev. A* **79**, 063631 (2009).

[33] Sakaguchi H. and Malomed B. A., Suppression of the quantum collapse in an anisotropic gas of dipolar bosons, *Phys. Rev. A* **84**, 033616 (2011).

[34] Tribelsky M. I., Exact solutions to fall of particle to singular potential: classical versus quantum cases, *Proc. R. Soc. A* **479**, 20230366 (2023).

[35] Bergé L., Wave collapse in physics: principles and applications to light and plasma waves, *Phys. Rep.* **303**, 259-370 (1998).

[36] Kuznetsov E. A. and Dias F., Bifurcations of solitons and their stability, *Phys. Rep.* **507**, 43-105 (2011).

[37] Fibich G., *The Nonlinear Schrödinger Equation: Singular Solutions and Optical Collapse* (Springer, Heidelberg, 2015).

[38] Sakaguchi H., Li B., and Malomed B. A., Creation of two-dimensional composite solitons in spin-orbit-coupled self-attractive Bose-Einstein condensates in free space, *Phys. Rev. E* **89**, 032920 (2014).

[39] Dodd R. J., Burnett K., Edwards M., and Clark C. W., Excitation spectroscopy of vortex states in dilute Bose-Einstein condensed gases, *Phys. Rev. A* **56**, 587-590 (1997).

- [40] Alexander T. J. and Bergé L., Ground states and vortices of matter-wave condensates and optical guided waves, *Phys. Rev. E* **65**, 026611 (2002).
- [41] Carr L. D. and Clark C. W., Vortices in attractive Bose-Einstein condensates in two dimensions, *Phys. Rev. Lett.* **97**, 010403 (2006).
- [42] Mihalache D., Mazilu D., Malomed B. A., and Lederer F., Vortex stability in nearly-two-dimensional Bose-Einstein condensates with attraction, *Phys. Rev. A* **73**, 043615 (2006).
- [43] Bogolyubov, N. N., On the theory of superfluidity, *Izv. Akad. Nauk SSSR, Ser. Fiz.* **11**, 77-90 (1947).
- [44] Kapitula T. and Promislow K., *Spectral and Dynamical Stability of Nonlinear Waves*, Springer-Verlag (New York, 2013).
- [45] Sadaka G., Jolivet P., Charalampidis E.G., and Danaila I., Parallel finite-element codes for the Bogoliubov-de Gennes stability analysis of Bose-Einstein condensates, *Comput. Phys. Commun.* **306**, 109378 (2025).